Chapter 7
Acceptor-Assisted Intraband Photoconductivity in $GaAs/AlGaAs$ Quantum Wells

Maxim Vinnichenko, Ivan Makhov, Vadim Panevin, Ratmir Ustimenko, Grigorii Melentev, Sergey Sorokin, Irina Sedova, David Hayrapetyan, and Dmitry Firsov

Abstract The present work is devoted to the experimental investigation of the far-, mid- and near-infrared photoconductivity related to the optical hole transitions involving acceptor states in $GaAs/AlGaAs$ quantum wells. Photoconductivity spectra are studied at low lattice temperatures. It is shown that the main contribution to the far- and mid-infrared photoconductivity is associated with the optical hole transitions from the ground acceptor state to the delocalized states of the valence subbands, delocalized states above the quantum well and to the excited states of the acceptors. The relaxation times of impurity-assisted photocurrent in quantum wells were also studied. The ionization energies of the acceptor impurity obtained by various experimental methods are in a good agreement with theoretical calculations.

7.1 Introduction

Technological progress in opto- and nanoelectronics allows to develop devices operating in the near-, mid- and far-infrared (IR) spectral ranges for a wide range of applications. Far-IR radiation can pass through a large number of different non-conducting materials. This feature of radiation gives a promising list of applications for devices based on it, for example, spectroscopy, astronomy, physical research of materials, medicine and security systems, etc. [1]. The mid-infrared spectral range as well as far-infrared one contains a large number of absorption lines of various gases

M. Vinnichenko (✉) · V. Panevin · R. Ustimenko · G. Melentev · D. Firsov
Peter the Great St. Petersburg Polytechnic University, St. Petersburg 195251, Russia
e-mail: mvin@spbstu.ru

I. Makhov
National Research University Higher School of Economics, St. Petersburg 194100, Russia

S. Sorokin · I. Sedova
Ioffe Institute, St. Petersburg 194021, Russia

D. Hayrapetyan
Russian-Armenian University, Yerevan 0051, Armenia

© The Author(s), under exclusive license to Springer Nature Switzerland AG 2022

D. Blaschke et al. (eds.), *Optics and Its Applications*, Springer Proceedings in Physics 281, https://doi.org/10.1007/978-3-031-11287-4_7

and molecules that are important for gas and bio sensing technologies. In accordance with the above, the development of sources and detectors operating in far- and mid-infrared spectral ranges is a promising task nowadays.

To date, the most efficient and compact source of far- and mid-infrared radiation is a quantum cascade laser [2, 3]. It has high enough output power, a fairly high efficiency and, most importantly, it has a small physical size. Despite the fact that quantum cascade lasers have several serious disadvantages, such as the complexity of the technological manufacturing and, accordingly, the high cost, they remain the most promising far- and mid-IR radiation sources.

The most well-proven detectors of far- and mid-IR radiation realized on semiconductors are based on intersubband optical transitions of charge carriers in 2D nanostructures with quantum wells (so-called quantum well infrared photodetectors (QWIP) [4, 5]) and interband optical transitions in bulk materials. The main difficulty with using QWIPs is associated with the need to fulfill the conditions of the selection rules for intersubband optical transitions according to which intersubband optical transitions of charge carriers can occur only for the light polarized along the growth axis of the structure. As a result, it leads to a complication of the photodetector structure design. Mid- and far-infrared photodetectors based on interband transitions are realized on semiconductors with a very narrow energy gap, such as $In_xAs_{1-x}Sb$ [6] and $Hg_xCd_{1-x}Te$ [7] alloys. Having a high sensitivity such alloys are difficult to grow as well as difficult to achieve the required doping profiles.

On the other hand, detection of infrared radiation can be realized with the use of charge carrier transitions involving impurity states. For example, the effective detection of far- and mid-infrared radiation is realized with bulk $Ge:Ga$ and $Ge:Hg$ photoresistors, respectively. The properties of impurities in bulk materials are comprehensively investigated to date. However, the energy spectrum of a certain impurity in a bulk semiconductor remains unchanged without external influences. In quantum well (QW) structures binding energy of an impurity center can be significantly varied by changing the QW parameters. The position of the impurity center in QW and the width of QW affect the energy spectrum of the impurity center [8]. Thus, doped QWs could expand the operating spectral range of devices based on impurity-related optical transitions. There is a significant amount of works related to the investigation of optical and photoelectrical properties of heterostructures with QWs doped with donor impurity centers. For example, far-infrared absorption [9, 10], photoconductivity [11, 12] and photoluminescence [12–15] are studied in $GaAs/AlGaAs$ quantum wells doped with shallow donors.

The optical properties of acceptors in QWs have not been studied in detail due to the non-trivial energy spectrum of acceptor and valence subband states. However, this feature allows to significantly expand the spectral range in which various acceptor-related optical phenomena can be observed. Moreover, p-type QWs have several advantages over n-type QWs. Firstly, acceptors have higher binding energy, it can even exceed the energy of optical phonons in $GaAs$. This can significantly increase the lifetime of photoexcited charge carriers, which is important for the development of mid- and far-infrared photodetectors. Secondly, according to the selection rules, intersubband optical transitions in p-type QWs are possible for radiation with a

polarization vector lying in the plane of the QW layers. This makes devices based on such structures promising for detectors and modulators of infrared radiation [16].

The present work is devoted to the experimental investigation of the infrared photoconductivity related to the optical hole transitions involving acceptor states in $GaAs/AlGaAs$ quantum wells.

7.2 Samples and Methods

200 $GaAs/Al_{0.4}Ga_{0.6}As$ quantum wells were MBE grown on a semi-insulating GaAs substrate. Each QW was 3 nm wide; the barriers between QWs were 7 nm wide. The central part of each QW ($\sim$ 0.7 nm) was doped with beryllium (acceptor) with a surface concentration of about 10^{11} cm^{-2}. For photoconductivity studies, the ohmic indium contacts were deposited on the sample surface. The contacts were annealed in a dry nitrogen atmosphere with smooth heating of the sample to 450 °C for 5 minutes, then this temperature was maintained for 5 min, and then sample was cooled to the room temperature for 5 min. The distance between the contacts was 5.1 mm, the length of the contacts was 5.8 mm.

The results of numerical calculations of the energy spectrum of acceptor states and valence subbands of the structure under study were previously presented by us in [17]. The system of differential equations for bulk semiconductors can be solved analytically, but for the case under study with QW, the eigenvalues of the Hamiltonian can be obtained only numerically, for example, by the finite difference method [18] or using the transfer matrix formalism [19]. In [17], well-proven methods were used for determining the energy of impurity levels by solving the Schrödinger equation with the Luttinger-Kohn Hamiltonian with the addition of the confining potential of the quantum well and the energy of the Coulomb interaction with a charged acceptor [20]. The calculated energy spectrum of valence subbands and acceptor states for a 3 nm wide $GaAs/Al_{0.4}Ga_{0.6}As$ QW is shown in Fig. 7.1. In the calculations, it was assumed that the impurity is located in the center of the QW. In [19] the momentum-dependent decomposition coefficients were used to calculate the optical matrix elements of the hole transitions from localized acceptor states to higher energy states in QW in dipole approximation. Calculated spectral and polarization dependencies of the infrared optical absorption due to photoionization of acceptors were verified by experimentally measured impurity-assisted absorption for two polarizations of light [17]. In this work, we continue the investigations of impurity-assisted optical transitions in p-doped $GaAs/Al_{0.4}Ga_{0.6}As$ quantum wells started in [17].

Experimental studies were performed using the Bruker Vertex 80v vacuum Fourier transform spectrometer operating in a rapid- or step-scan mode (see scheme of the experiment presented in Fig. 7.2) with spectral resolution of about 1 meV. The spectrometer was equipped with a Mylar, KBr or CaF_2 beam splitters (BMS) for the far-infrared, mid-infrared and near-infrared studies, respectively. A globar was used as a source of broadband infrared radiation. For good heat dissipation, the sample

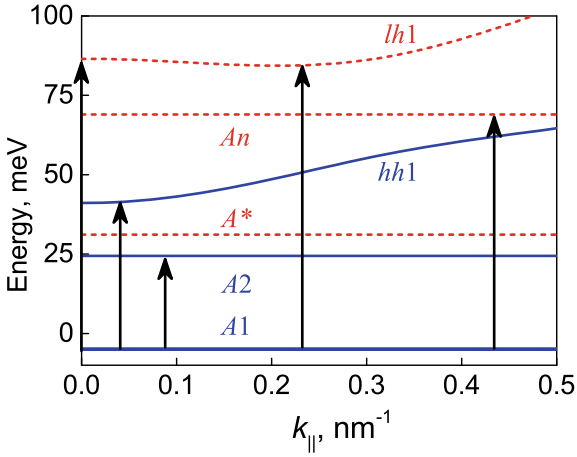

Fig. 7.1 Calculated energy spectrum of acceptor states and valence band subbands for a $GaAs/Al_{0.4}Ga_{0.6}As$ QW of 3 nm wide. Blue curve corresponds to the first hole subband (hh—heavy holes), and red one corresponds to the second hole subband (lh—light holes). The extension of impurity levels is shown schematically with solid and dashed horizontal lines without considering the degree of localization of impurity states in the k-space

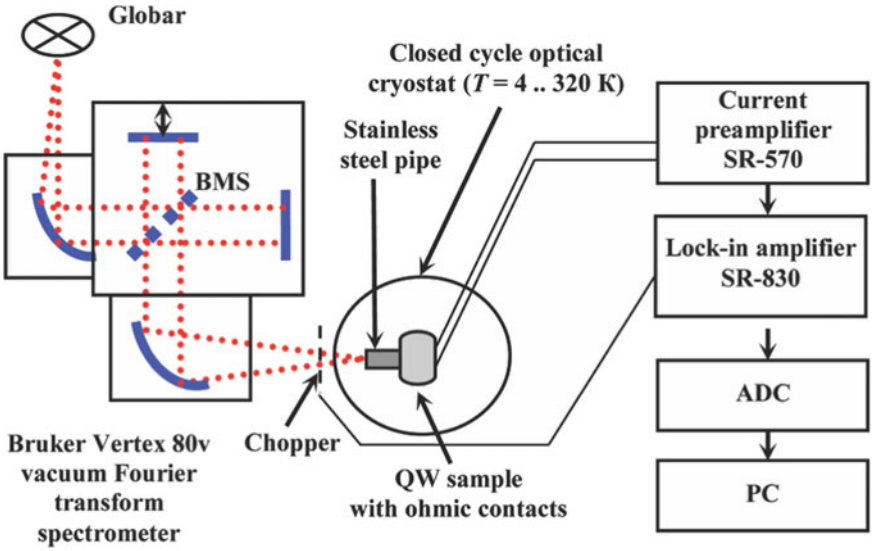

Fig. 7.2 Experimental setup scheme for investigation of the photoconductivity spectra

was indium-soldered to a copper holder of a Janis PTCM-4-7 closed-cycle optical cryostat with an operating temperature range of 4 – 320 K. The entrance window of the cryostat was made of KBr or TPX for mid-infrared and far-infrared stud-

ies, respectively. The sample in the cryostat was shielded all around from external background radiation to prevent undesirable photoionization of impurities.

Photoconductivity measurements were carried out under 5 V bias voltage applied to the sample using a SR-570 current preamplifier. The light from the globar passed through the interferometer of the Fourier spectrometer and then was modulated with an optical chopper. Infrared radiation was directed to the sample through a cold polished stainless steel pipe of a 5 mm diameter. A chopper was synchronized with lock-in amplifier SR-830. The photocurrent from the sample was registered by the above-mentioned SR-570 current preamplifier, and then measured by lock-in amplifier SR-830. This signal after analog-digital converter (ADC) was accumulated in personal computer (PC), where obtained interferogram was converted to spectrum by Fourier transform in OPUS software.

7.3 Experimental Results

7.3.1 Photoconductivity Spectra

The interband photoconductivity spectra of the $GaAs/Al_{0.4}Ga_{0.6}As$ quantum well structure in the near-IR spectral range at various cryogenic temperatures are shown in Fig. 7.3. The photocurrent increases at the photon energy close to the $GaAs$ energy gap value, which corresponds to the interband transitions of charge carriers in $GaAs$ (marked with arrow E_g in Fig. 7.3). It is associated with the contribution to the photocurrent from the $GaAs$ substrate and the $p-GaAs$ cap layer of the nanostructure. We observed in the photoconductivity spectra two dips corresponding to the photon energies of optical transitions associated with formation of heavy hX and light lX free excitons in QW (the corresponding photon energies are shown with arrows in Fig. 7.3). Photon energy values for these optical transitions were obtained using free heavy and light exciton binding energies as 10 meV and 13 meV, respectively, calculated in [21]. Spectral position of heavy free exciton line was also verified by low-temperature near-infrared photoluminescence studies (see inset to Fig. 7.3). These excitons are formed by charge carriers located in the ground QW subbands. The total photocurrent of the structure decreases at the hX and lX photon energies at rather low crystal lattice temperatures because excitons with such high binding energies cannot contribute to the photocurrent. The positive contribution of excitons to the photocurrent may be observed at higher lattice temperatures, when the energy of thermal motion of charge carriers is comparable to the binding energy of the exciton. In this case, the excitons formed under the action of radiation can contribute to the photocurrent due to thermal dissociation into a nonequilibrium electrons and holes in the subbands of the conduction and valence bands. The luminescence band related to the optical transitions of electrons from the first electron subband to the ground acceptor state was also observed in the near-infrared photoluminescence spectrum (see inset to Fig. 7.3). The arrow $e1-A1$ in inset to Fig. 7.3 shows the

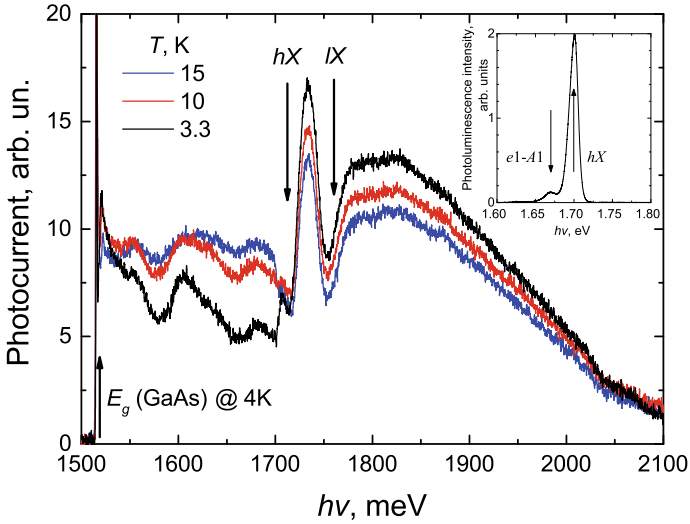

Fig. 7.3 Spectra of interband near-infrared photoconductivity at different temperatures. The inset shows near-infrared photoluminescence spectrum measured at $T = 4$ K

calculated position of the energy of optical electron transition from the first electron subband to the ground state of acceptor impurity. It should be noted that contribution of the optical transitions of charge carriers from the acceptor states to the first electron subbands was not revealed in the near-infrared photoconductivity spectra because in equilibrium the acceptor states are unoccupied by electrons at low crystal lattice temperatures.

The long-wavelength part of the photoconductivity spectra (photon energy below 1700 meV) is related to the charge carriers generated in the near-surface heavily doped (near the critical acceptor concentration for Mott transition) $GaAs$ cap layer as well as in semi-insulating compensated $GaAs$ substrate, which contains substantial concentration of ionized donors. At low temperatures, ionized impurity scattering is the main scattering mechanism indoped $GaAs$ [22]. With increasing temperature, the intensity of the impurity scattering decreases, which leads to an increase in the mobility of photoexcited charge carriers and to an increase in photoconductivity with temperature. The inverse temperature dependence of photoconductivity at high photon energies (photon energies above 1750 meV) can be explained by the fact that layers with quantum wells make a significant contribution to photoconductivity in this spectral region. At low temperatures, the acceptors in quantum wells are non-ionized and the mobility of charge carriers is determined by phonon scattering, the intensity of which increases with temperature.

The impurity-assisted time-resolved photoconductivity spectra were measured in step-scan mode of Fourier-spectrometer in mid-infrared spectral range. The time-resolved photoconductivity spectra at $T = 4$ K are shown in Fig. 7.4. Photoconductivity spectra at the liquid helium temperature were also measured in rapid scan mode

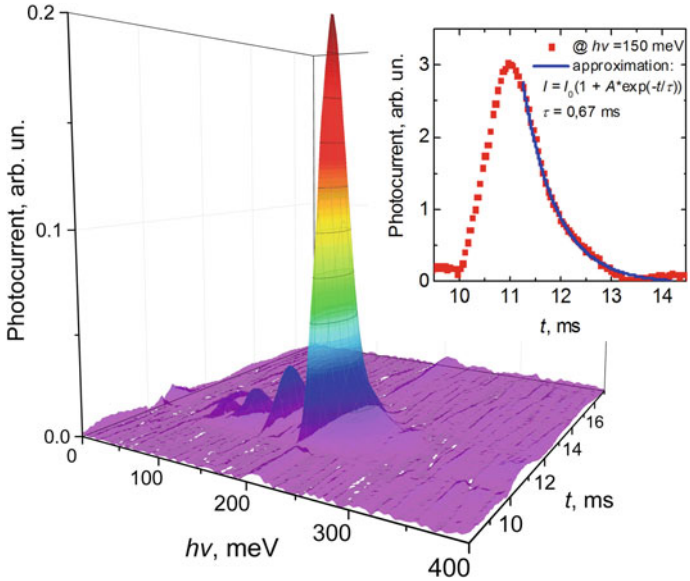

Fig. 7.4 Time-resolved spectra of impurity-assisted photoconductivity in the mid-IR range at $T = 7$ K. Inset: photocurrent dynamic at the photon energy of 150 meV

of the Fourier-transform spectrometer for different values of scanning velocity f of the interferometer. The results are shown in the Fig. 7.5. It should be noted that current preamplifier bandwidth was of about 1 MHz. The wide peak observed near the photon energy of 205 meV is associated with the optical transitions of holes from the ground acceptor state $A1$ to the continuum states above the QW. The small shoulder in the photocurrent at a photon energy of about 240 meV could be associated with the contribution of deep impurity centers in the layers of the nanostructure to the photocurrent [23] or with some features of joint density of states for hole transitions. We associate the photocurrent peak at the photon energy of about 150 meV with optical transitions of holes from the ground impurity state $A1$ to the bottom of the third hole subband (or the second subband of heavy holes $hh2$, which is not shown in Fig. 7.1). It is important to note that in the calculation presented in Fig. 7.1, we used the expansion of the hole wave function in the states of the first two valence subbands only. So, in order to obtain third hole subband $hh2$ we used the standard solution of the Schrödinger equation in the framework of the parabolic model. The photocurrent peak at the photon energy of about 90 meV (see Fig. 7.5) is associated with the optical transitions of holes from the ground state of acceptor impurity $A1$ to states near the bottom of the second hole subband $lh1$ near $k_{\parallel} = 0$ (arrow $A1 - lh1$ in Fig. 7.1). In general, from Fig. 7.5 it is clearly seen that with an increase in the scanning speed of the interferometer, the intensity of the photocurrent decreases. It is connected with finite relaxation time of holes from the valence subbands and excited impurity states to the ground impurity states. This time is estimated as a few mil-

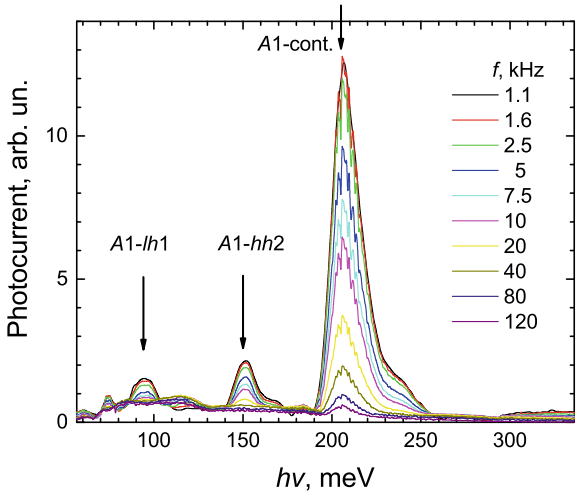

Fig. 7.5 Impurity-assisted photoconductivity spectra in the mid-IR range at $T = 7$ K for different scanning velocity f of interferometer

liseconds. Also, this time can be obtained from the time-resolved spectrum (see Fig. 7.4). We approximated the photocurrent dynamics (see inset to Fig. 7.4 for photon energy of about 150 meV) with an expression derived from the rate equation:

$$I = I_0 \left(1 + A \cdot \exp\left(t/\tau\right)\right), \tag{7.1}$$

where I—photocurrent intensity; I_0 and A—fitting parameters; τ—relaxation time. Using this approximation method, we got relaxation times for three observed optical transitions in the range of 0.58–0.67 ms. The obtained relaxation time for the acceptor-related optical transitions is quite large. It can be related to the large binding energy of acceptors in our 3 nm wide quantum wells. The calculated value of acceptor binding energy is about 40 meV, that exceeds the $GaAs$ optical phonon energy resulting in a significant suppression of the carrier capture to acceptor with optical photon scattering. It also should be noted that in semi-insulating $GaAs$, the relaxation time for optical transitions of electrons from the conduction band to the ground acceptor state at low crystal lattice temperatures is about tens microseconds or more [24].

We also measured the spectra of impurity-assisted photoconductivity in the mid-IR spectral range for different cryogenic temperatures from 4 K with a step of 2 K. All photocurrent peaks gradually decrease and at a temperature of about 30 K the photocurrent disappears due to impurity ionization. The reference samples without QWs did not exhibit any features in the photocurrent spectra. This confirms that all the features observed in the mid-infrared photoconductivity spectra of QWs are associated with impurity transitions in QWs and agrees well with theoretical calculations.

The far-infrared impurity-assisted photoconductivity spectra are shown in the Fig. 7.6 for different lattice temperatures. The wide long-wavelength peak near a photon

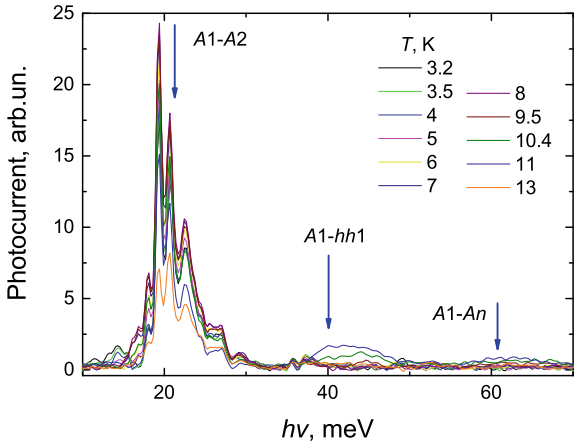

Fig. 7.6 Impurity-assisted photoconductivity spectra in the far-infrared spectral range at different temperatures

energy of about 20 meV is associated with the optical hole transitions from the ground acceptor state $A1$ to the first excited state of the acceptor $A2$ (arrow $A1 - A2$ in Fig. 7.1). These excited carriers in $A2$ state can contribute to the photocurrent due to thermal ejection into the first subband of the valence band $hh1$. The peak in photoconductivity spectra located near the photon energy of about 40 meV could be associated with the hole transitions from the ground state of the acceptor impurity $A1$ to the first subband of heavy holes $hh1$, which also agrees well with the calculated value of the acceptor binding energy (arrow $A1 - hh1$ in Fig. 7.1). The photocurrent peak at the photon energy of about 60 meV is associated with intracenter optical transitions of holes between the ground state of the impurity $A1$ and the impurity states located below the second hole subband $lh1$ (arrow $A1 - An$ in Fig. 7.1). All photocurrent peaks gradually decrease with temperature and at the temperature of about 15 K the photoconductivity disappear due to impurity ionization.

7.3.2 Temperature Dependence of Electroconductivity

It was shown above that investigations of photoconductivity have confirmed our calculation of the energy spectrum of impurity states and the band diagram of QWs. Additionally, we have determined the binding energy of acceptors in the QW from the analysis of the temperature dependence of the electroconductivity σ (see red dots in Fig. 7.7). Firstly, we assumed that electroconductivity is proportional to the concentration of ionized holes in the valence band. This is correct if the hole mobility is assumed to be temperature independent. Secondly, it was important to consider that hole gas is non-degenerate. To prove this, let's find the temperature dependence of the concentration. In the impurity conductivity range, two-dimensional concentration of ionized holes in the valence band n_s can be written as [25]

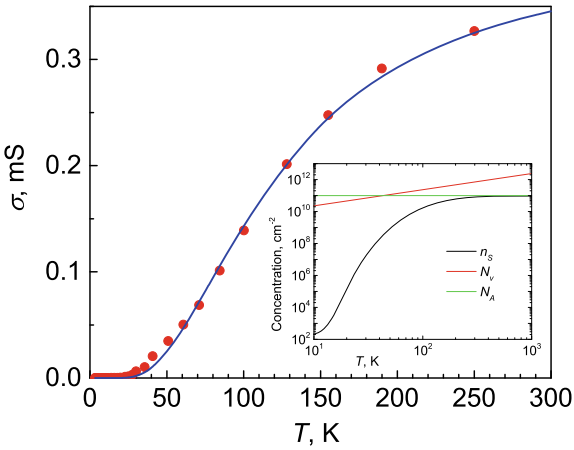

Fig. 7.7 Temperature dependence of electroconductivity. Red dots—experimental data, blue line—theoretical calculations according to Eq. (7.6). Inset: calculated temperature dependence of two-dimensional concentration of ionized holes in the valence band n_s, N_V—effective density of states in valence subband, N_A—concentration of acceptors

$$n_s = N_A - N_h, \tag{7.2}$$

where N_A—concentration of acceptors, N_h—concentration of unionized holes at the impurity levels. The hole concentration at acceptor levels according to the Fermi statistics is

$$N_h = \frac{N_A}{1 + \beta \exp\left(\frac{-E_A - \mu}{kT}\right)}, \tag{7.3}$$

where β—impurity degeneracy factor of the ground acceptor state, equal to 4 for holes in the QW; E_A—ionization energy of an acceptor impurity; μ—Fermi energy. Substituting expression (7.3) into (7.2) one can obtain the Fermi energy

$$\mu = -E_A - kT \ln\left(\frac{n_s}{N_h \beta}\right), \tag{7.4}$$

It is also known that for the two-dimensional Fermi-Dirac statistics, Fermi energy can be written as

$$\mu = kT \ln\left(\exp\left[\frac{n_s}{N_V}\right] - 1\right), \tag{7.5}$$

where $N_V = mkT/\left(\pi\hbar^2\right)$ is the two-dimensional effective density of states in valence subband, m—effective mass of holes. Equating μ from (7.4) and (7.5), we obtain the relationship between concentration of ionized holes in the valence band n_s and temperature with E_A as parameter

$$\exp\left(\frac{E_A}{kT}\right) = \frac{n_s}{(N_A - n_s)\beta}\left(\exp\left[\frac{n_s}{N_V}\right] - 1\right), \tag{7.6}$$

Using Eq. (7.6) and assuming that $\sigma(T) \sim n_s(T)$ we plotted dependence $\sigma(T)$ (see blue line in Fig. 7.7) with fitting parameter $E_A = 40$ meV. It gives the best fit between the experimental and calculated data. Also, from Eq. (7.6) we received dependence $n_s(T)$ (see black line in the inset to Fig. 7.7). One can see that concentration of free holes n_s is much less than the effective density of states N_V in the hole subband. This confirms that the hole gas is non-degenerate.

The value of the acceptor ionization energy obtained from $\sigma(T)$ is compatible with calculated one (see Fig. 7.1) and with values obtained from near-infrared photoluminescence (see inset to Fig. 7.3) and far-infrared photoconductivity studies (see Fig. 7.6). Also, the obtained ionization energy of acceptors in the QW is in a good agreement with the results of other authors [26, 27].

7.4 Conclusion

The results of studies of low-temperature acceptor-assisted photoconductivity of $p - GaAs/AlGaAs$ QW were presented in the near-, mid- and far-infrared spectral ranges. The mid- and far-infrared photoconductivity spectra contain the bands associated with the hole transitions from the ground acceptor state to the delocalized states of the valence subbands, delocalized states above the QW and to the excited states of the acceptor. The features of near-infrared photoluminescence and photoconductivity spectra are related to the interband optical transitions with assistance of impurities as well as with exciton transitions. Time-resolved photoconductivity spectra allowed us to find the relaxation time of impurity-assisted transitions. The ionization energies of the acceptor impurity determined by various experimental methods are in a good agreement with theoretical calculations.

Acknowledgements The work was partially funded by the Ministry of Science and Higher Education of the Russian Federation as part of thematic work "Activities to support of efficiency of Russian-Armenian and Belorussian-Russian Universities" (supplement agreement contract No. 075-03-2021-050/5 dated 08.07.21). Also, work was partially supported by the Russian Science Foundation under grant No. 18-72-00034 and the Ministry of Science and Higher Education of the Russian Federation (state assignment No. 075-03-2021-050). IM acknowledges support from the Basic Research Program of the National Research University Higher School of Economics.

References

1. Tonouchi, M.: Cutting-edge terahertz technology. Nat. Photon. **1**, 97–105 (2007)
2. Bosco, L., et al.: Thermoelectrically cooled THz quantum cascade laser operating up to 210 K. Appl. Phys. Lett. **115**, 010601 (2019)
3. Razeghi, M., et al.: Quantum cascade lasers: from tool to product. Opt. Express **23**(7), 8462–8475 (2015)
4. Gueriaux, V., et al.: Quantum well infrared photodetectors: present and future. Opt. Eng. **50**(6), 061013 (2011)

5. Liu, H.C., Song, C.Y., SpringThorpe, A.J., Cao, J.C.: Terahertz quantum-well photodetector. Appl. Phys. Lett. **84**(20), 4068–4070 (2004)
6. Rogalski, A., et.al.: InAsSb-based infrared photodetectors: Thirty years later on. Sensors (Switzerland) **20**(24), 7047, 1–74 (2020)
7. Rogalski, A.: HgCdTe infrared detector material: history, status and outlook. Rep. Prog. Phys. **68**(10), 2267–2336 (2005)
8. Masselink, W.T., et al.: Shallow impurity levels in AlGaAs/GaAs semiconductor quantum wells. Solid-State Electron. **29**(2), 205–214 (1986)
9. Jiang, P., Kok, W.C.: Far-infrared absorption spectra of doped quantum well structures. J. Appl. Phys. **90**(3), 1271–1274 (2001)
10. Helm, M., et al.: Far-infrared spectroscopy of minibands and confined donors in GaAs/AlxGa1-xAs superlattices. Phys. Rev. B **43**(17), 13983–13991 (1991)
11. Mercy, J.M., Jarosik, N.C., McCombe, B.D. Photoconductivity of confined donors in Al0.3Ga0.7As/GaAs quantum wells. J. Vacuum Sci. Technol. B Microelectron. Process. Phenom. **4**, 1011–1013 (1986)
12. Firsov, D.A., et al.: Terahertz emission and photoconductivity in n-type GaAs/AlGaAs quantum wells: the role of resonant impurity states. Semiconductors **44**(11), 1394–1397 (2010)
13. Makhov, I.S., et al.: Terahertz photoluminescence of the donor doped GaAs/AlGaAs quantum wells controlled by the near-infrared stimulated emission. J. Lumin. **210**, 352–357 (2019)
14. Makhov, I.S., et al.: Impurity-assisted terahertz photoluminescence in compensated quantum wells. J. Appl. Phys. **126**(17), 175702 (2019)
15. Makhov, I.S., et al.: The effect of stimulated interband emission on the impurity-assisted far-infrared photoluminescence in GaAs/AlGaAs quantum wells. Superlattices Microstruct. **112**, 79–85 (2017)
16. Chen, H.H., Wang, Y.-H., Houng, M.-P.: Near 10 μm intervalence sub-band optical transitions in p-type In0.49Ga0.51P-GaAs quantum well structures. IEEE J. Quant. Electron. **32**(3), 471–477 (1996)
17. Vinnichenko, M.Ya. et. al.: Acceptor-related infrared optical absorption in GaAs/AlGaAs quantum wells. Phys. E: Low-dimensional Syst. Nanostruct. **124**, 114601 (2020)
18. Ikonić, Z.: Milanović, V: Hole-bound-state calculation for semiconductor quantum wells. Phys. Rev. B **45**(15), 8760–8762 (1992)
19. Tadić, M., Ikonić, Z.: Bound-free intersubband absorption in p-type doped semiconductor quantum wells. Phys. Rev. B **52**(11), 8266–8275 (1995)
20. Brown, G.J. et. al.: Intersubband hole absorption in GaAs-GaInP quantum wells grown by gas source molecular beam epitaxy. Appl. Phys. Lett. **65**(9), 1130–1132 (1994)
21. Belov, P.A.: Energy spectrum of excitons in square quantum wells. Physica E **112**, 96–108 (2019)
22. Blakemore, J.S.: Semiconducting and other major properties of gallium arsenide. J. Appl. Phys. **53**, R123–R181 (1982)
23. Bourgoin, J.C., Von Bardeleben, H.J., Stievenard, D.: Native defects in gallium arsenide. J. Appl. Phys. **64**(9), R65–R92 (1988)
24. Kurdyubov, A.S. et. al.: Impurity-induced modulation of terahertz waves in optically excited GaAs. AIP Adv. **7**(11), 115222 (2017)
25. Blakemore, J.S.: Semiconductor Statistics. Courier Corporation (2002)
26. Masselink, W.T., Chang, Y.C., Morkoc, H.: Acceptor spectra of AlxGa1-xAs-GaAs quantum wells in external fields: electric, magnetic, and uniaxial stress. Phys. Rev. B **32**(8), 5190–5201 (1985)
27. Einevoll, G.T., Chang, Y.C.: Effective bond-orbital model for shallow acceptors in $GaAs - Al_xGa_{1-x}As$ quantum wells and superlattices. Phys. Rev. B **41**(3), 1447–1460 (1990)